Comparative Study of the Effect of Different Nanoparticles on the Mechanical Properties, Permeability, and Thermal Degradation Mechanism of HDPE

K. Chrissafis,[1] K. M. Paraskevopoulos,[1] I. Tsiaoussis,[1] D. Bikiaris[2]

[1]*Solid State Physics Section, Physics Department, Aristotle University of Thessaloniki, Thessaloniki GR- 541 24, Macedonia, Greece*
[2]*Laboratory of Organic Chemical Technology, Department of Chemistry, Aristotle University of Thessaloniki, ThessalonikiGR-541 24, Macedonia, Greece*

Received 17 February 2009; accepted 6 May 2009
DOI 10.1002/app.30750
Published online 23 June 2009 in Wiley InterScience (www.interscience.wiley.com).

ABSTRACT: In the present study, different series of high-density polyethylene (HDPE) nanocomposites were prepared by melt mixing on a Haake-Buchler Reomixer, containing 2.5 wt % of multiwall carbon nanotubes, pristine and modified montmorillonite, surface-treated and -untreated SiO_2 nanoparticles. From transmission electron micrographs, it was found that beyond a fine dispersion of nanoparticles into HDPE matrix, there are also some aggregates easily discriminated. As a result, there was a decrease in the tensile and impact strength of most of nanocomposites except Young's modulus, which was increased. Storage modulus as recorded from dynamic mechanical analysis was also increased in all nanocomposites, because HDPE becomes stiffer due to the incorporation of nanoparticles. The nucleation behavior of nanoparticles during crystallization was found to have no obvious effect on melting and crystallization temperature of HDPE. However, a small decrease in the heat of fusion in all nanocomposites was evidenced. Gas permeability of HDPE matrix in O_2, N_2, and CO_2 was reduced in all nanocomposites compared with neat polymer. Thermal stability of HDPE was also enhanced due to the incorporation of different nanoparticles. From the kinetic analysis of thermal decomposition of HDPE, it was concluded that to describe the thermal degradation of HDPE and the studied nanocomposites, two consecutive mechanisms of *n*th-order autocatalysis have to be considered. J Appl Polym Sci 114: 1606–1618, 2009

Key words: nanocomposites; polyethylene; multiwalled carbon nanotubes; montmorillonite; fumed silica; thermal stability; gas permeability

INTRODUCTION

Among the wide number of commercially available thermoplastic polymers, high-density polyethylene (HDPE) has been widely used in different packaging applications. This is due to the abundant supply of HDPE and to its combination of low-cost and low-energy demand for processing. Additionally, the well-balanced mechanical properties make HDPE ideal for many industrial applications.[1] The introduction to the market of HDPE with bimodal molecular weight distribution has extended its applications such as production of pipes and fittings for the transportation of water or gas under pressure. The high molecular weight part gives materials with increased mechanical properties, whereas the low molecular weight part acts as lubricant during HDPE extrusion. Referring to mechanical properties, HDPE, compared with the other kinds of polyethylene, has very high tensile strength due to its highly crystalline structure. On the other hand, for gas transportation pipes as well as for food and drug packaging, gas permeability is one of the most important properties to be considered. HDPE offers a good barrier for humidity but is easily permeated by oxygen. Some of these properties can be improved by the addition of inorganic particles into polymer matrices. In conventional composites, a large amount of fillers (>20 vol %) of microparticle size is, generally, required to appreciably increase the elastic modulus and reduce the creep compliance of thermoplastic matrices.[2] However, these gains are usually accompanied by severe losses in many other properties and especially, the ductility and toughness. From the other side, polymers filled with nanoparticles have attracted great interest nowadays, both in industrial and academic areas.

The nanocomposites are characterized by the use of a reinforcing agent with nanodimensions, which is added in small quantities compared with the traditional composites. In these nanocomposites, the addition of relatively small amounts (<3 vol %) of

Correspondence to: D. Bikiaris (dbic@chem.auth.gr).

inorganic particles, such as silica, titania, or calcium carbonate or carbon nanotubes, has been proven to increase both rigidity and toughness, thermal and barrier properties of different thermoplastics.[3] In this context, nanoparticles have a fundamental role in properties enhancement, compared with the pristine polymers, presumably due to the nanoscale structure of nanoparticles and the synergism between polymer and nanoparticles.

In the case of HDPE, several nanoparticles were used to increase its mechanical properties such as tensile modulus and impact strength.[4,5] SiO_2 nanoparticles[6] as well as montmorillonite (MMT) were reported to increase tensile strength and flame retardance of HDPE.[7] However, in most of the cases, it was reported that the addition of MMT causes a reduction in tensile strength and only Young's modulus increases.[8] Maleated polyethylene can be used to increase the dispersion of MMT nanoparticles into HDPE matrix and thus enhances its mechanical properties.[9–11] Except SiO_2 and MMT, multiwalled carbon nanotubes (MWCNTs) were also used for stiffness enhancement as well as increase of thermal conductivity of HDPE.[12–15] However, so far, only limited studies concerning the gas permeability improvement of HDPE by the addition of nanofillers were reported.[16,17]

In this study, several nanoparticles such as MMT, MWCNTs, and fumed silica were used to prepare HDPE/nanocomposites. These nanoparticles are extensively used to improve many of the polymer properties. The aim of this study was to evaluate the effect of the above-mentioned nanoparticles compared with the mechanical, gas permeability, and mainly to the thermal decomposition properties of HDPE using several kinetic models. For this reason, the nanoparticles amount was stable, 2.5 wt % in all nanocomposites, because from many studies it was found that, at such amount, the highest mechanical properties of nanocomposites can be achieved.

EXPERIMENTAL

Materials

Bimodal HDPE appropriate for pipe and fittings production was supplied by TVK Inter-Chemol GmbH (Frankfurt am Main, Germany) under the trade name TIPELIN 7700M and had a melt flow index of 0.28 g/10 min at 5.0 kg/190°C, density 0.950 g/cm^3 and T_m 127°C. MWCNTs used in this work were synthesized by the chemical vapor deposition process and were supplied by Nanothinx (Patra, Greece). Their diameter was between 9 and 20 nm and their length was $>$ 5 μm. The two different types of fumed silica (SiO_2) nanoparticles used for nanocomposites preparation were supplied by Degussa AG (Hanau, Germany). The first type was hydrophilic silica nanoparticles, under the trade name AEROSIL® 200, having a specific surface area of 200 m^2/g and SiO_2 content $>$99.8%, and the second type was the hydrophobic nanoparticles under the trade name AEROSIL R974. The latter were produced by the supplier after treating the hydrophilic nanoparticles with dimethyldichlorosilane ($cSiO_2$) and had lower specific surface than the untreated (170 m^2/g). In both the cases, the average primary particle size was 12 nm. The two different types of MMT under the trade name Cloisite® Na^+ (pristine) (MMT) and Cloisite 20A (org-MMT), which is modified with a dimethyl, dihydrogenated tallow quaternary ammonium chloride salt, were supplied from Southern Clay Products Inc. (Golzales, TX). The particle sizes of both montmorilonites range between 2 and 13 μm and have modulus of elasticity 4.657 GPa, tensile strength 101 MPa, and moisture content $<$2%.

Nanocomposites preparation

Nanocomposites containing 2.5 wt % of nanoparticles were prepared by melt mixing in a Haake-Buchler Reomixer (Model 600) with roller blades and a mixing head with a volumetric capacity of 69 cm^3. Five different types of nanoparticles were used such as MWCNTs, uncoated and coated SiO_2, pristine, and organically modified MMT. Before melt mixing, the nanoparticles were dried by heating in a vacuum oven at 130°C for 24 h. The two components were physically premixed before being fed in the reomixer, to achieve a better dispersion of the nanoparticles in HDPE. Melt blending was performed at 220°C and 30 rpm for 15 min. During the mixing period, the melt temperature and torque were continuously recorded. Each nanocomposite after preparation was milled and placed in a desiccator to prevent any moisture absorption.

Mechanical properties

Measurements of tensile mechanical properties of the prepared nanocomposites were performed on an Instron 3344 dynamometer, in accordance with ASTM D638, using a crosshead speed of 50 mm/min. Relative thin sheets of about 350 ± 25 μm were prepared using an Otto Weber, Type PW 30 hydraulic press connected with an Omron E5AX Temperature Controller, at a temperature of 190 ± 5°C. The molds were rapidly cooled by immersing them in water at 20°C. From these sheets, dumbbell-shaped tensile test specimens (central portions 5× 0.5 mm thick, 22-mm gauge length) were cut in a Wallace cutting press and conditioned at 25°C and 55–60% relative humidity for 48 h. The values of Young's

modulus, yield stress, elongation at break, and tensile strength at the break point were determined. At least five specimens were tested for each sample and the average values, together with the standard deviations, are reported.

Izod impact tests were performed using a Tinius Olsen apparatus in accordance with ASTM D256 method. Five measurements were conducted for each sample, and the results were averaged to obtain a mean value.

Dynamic mechanical analysis

The dynamic thermomechanical properties of the nanocomposites were measured with a Rheometric Scientific analyzer (Model Mk III). The bending method was used at a frequency of 1 Hz, a strain level of 0.04% in the temperature range of –100°C to 60°C. The heating rate was 3°C/min. Testing was performed using rectangular bars with dimensions, approximately, 30 × 10 × 3 mm. These were prepared with a hydraulic press, at a temperature of 190°C and a pressure of 100 bar, for a time period of 5 min. The exact dimensions of each sample were measured before the scan.

Transmission electron microscopy

Electron diffraction and transmission electron microscopy (TEM) observations were performed on ultra-thin film samples of the various nanocomposites, prepared by an ultramicrotome. These thin films were deposited on copper grids. A JEOL 120 CX microscope was used, operating at 120 kV.

Wide-angle x-ray diffractometry

Wide-angle x-ray diffractometry study of HDPE nanocomposites after crystallization for 10 days at 0°C were performed over the range 2θ from 5 to 55°, at steps of 0.05° and counting time of 5 seconds, using a Philips PW1710 powder diffractometer with CuK_α Nickel-filtered radiation.

Differential scanning calorimetry

Thermal analysis of the nanocomposites was performed using a differential scanning calorimeter (Setaram, DSC141) calibrated with indium and zinc standards. For each measurement, a sample of about 6.0 ± 0.2 mg was used, placed in a sealed aluminium pan, and heated to 180°C at a scanning rate of 5°C/min. From these scans, the melting temperature (T_m) of the nanocomposites was measured. Crystallization temperature (T_c) from the melt was also recorded by cooling the samples from 180 to 60°C at a cooling rate of 2.5°C/min.

Thermogravimetric analysis

Thermogravimetric analysis was carried out with an SETARAM SETSYS TG-DTA 16/18 instrument. Samples (6.0 ± 0.2 mg) were placed in alumina crucibles. An empty alumina crucible was used as reference. HDPE nanocomposites were heated from ambient temperature to 550°C in a 50 mL/min flow of N_2 at heating rates of 5, 10, 15, and 20°C/min. Continuous recordings of sample temperature, sample weight, its first derivative, and heat flow were taken.

Permeability studies

Permeability rates were studied on relatively thin films of HDPE nanocomposites, prepared as the films for the tensile measurements. To prepare films devoid of entrapped air bubbles, the load was gradually increased up to 10 kN during a time of 3 min and maintained at this load for additional 2 min. All prepared films had a thickness of approximately 50 ± 5 μm. Permeability rates of O_2 and N_2 through these films were measured using a Davenport Apparatus (London). For this reason, a dried No. 1 Whatman filter with a diameter of 5.5 cm was used to support the nanocomposite films. The apparatus was fixed and vacuum was applied to the lower part of the shell down to a pressure of <0.2 mmHg. After this, gas was introduced in the upper part of the apparatus shell and the pressure difference in a capillary pipe (cmHg h^{-1}) was measured against time until a constant rate was reached. From each sample, three measurements were completed and the results were averaged to obtain a mean value.

RESULTS AND DISCUSSION

Nanocomposites characterization

It is well known that most of the properties in polymer nanocomposite materials are directly dependent on the particle size distribution of nanoparticles into polymer matrix. Because of the high aspect ratio of nanoparticles, aggregates are usually formed that mainly reduce the mechanical properties. In this study, the morphology of the prepared nanocomposites is examined with TEM. As can be seen from Figure 1, TEM micrographs revealed that silica particles (coated and uncoated) were characterized by a spherical shape and narrow grain size distribution. Even though these nanoparticles consist of individual particles in the range of 12 nm, during melt mixing with HDPE aggregates are formed since the observed nanoparticles are in the range of 50–300 nm. This behavior has been also observed in other polyolefins.[18–22] Comparing the treated and untreated silica nanoparticles, it can be seen that those with surface treatment are producing

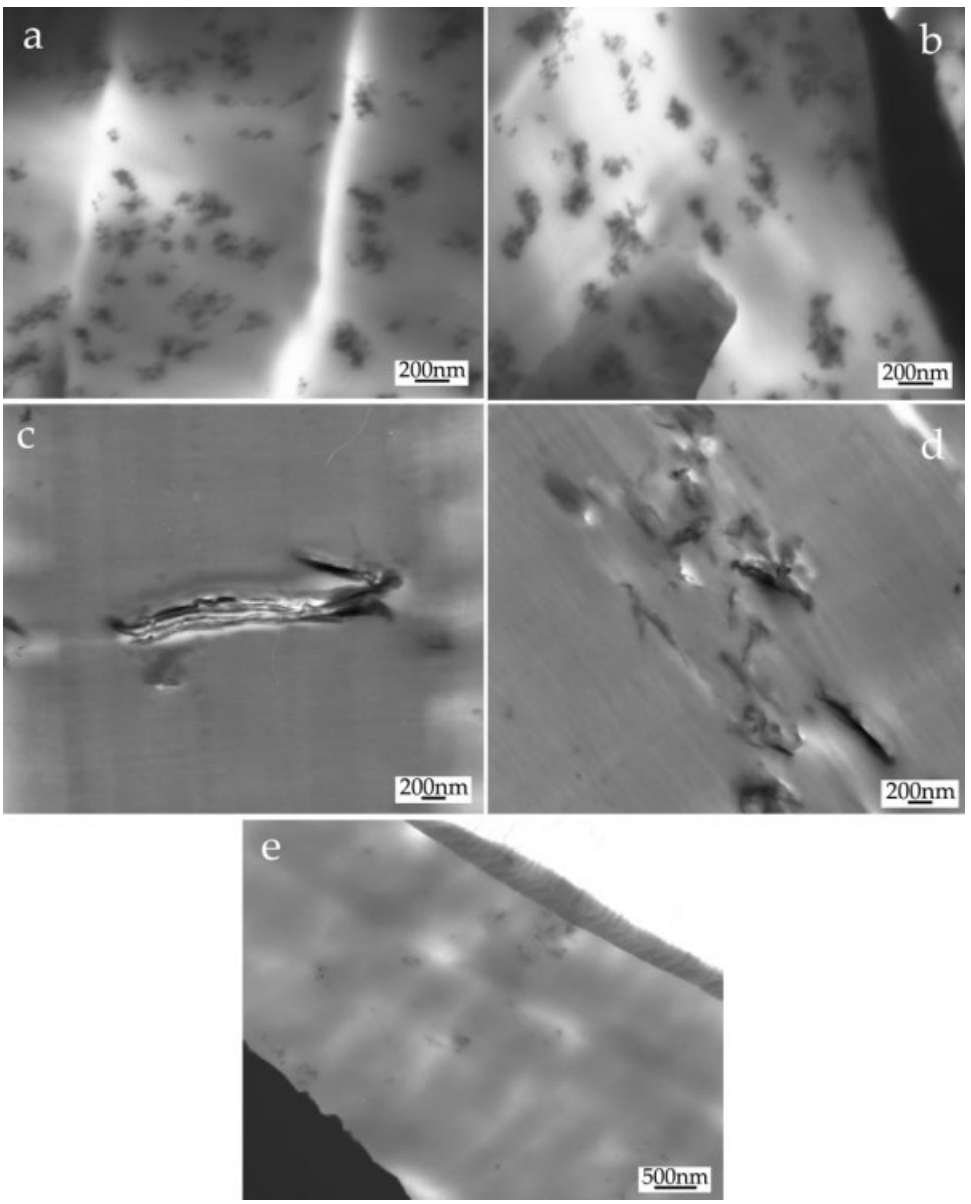

Figure 1 TEM micrographs of HDPE nanocomposites containing (a) SiO_2, (b) $cSiO_2$, (c) MMT, (d) org-MMT, and (e) MWCNTs.

aggregates with slightly higher sizes. This was also observed in our previous studies and maybe attributed to the larger initial particles of coated SiO_2 compared with uncoated SiO_2.[19,20] However, the differences are very small to extract any clear conclusion. In the case of HDPE/MMT nanocomposites,

TABLE I
Mechanical Properties of HDPE/Nanocomposites

Material	Tensile strength at Yield (MPa)	Tensile strength at break (MPa)	Young's Modulus (MPa)	Elongation at break (%)	Impact strength (J/m)
HDPE	19.7 ± 2.3	29.9 ± 2.4	609 ± 34	770 ± 45	42 ± 5
HDPE/MWCNTs	19.5 ± 2.9	13.6 ± 1.9	796 ± 42	54 ± 12	29 ± 3
HDPE/SiO_2	21.7 ± 2.5	33.8 ± 1.5	725 ± 25	776 ± 52	36 ± 4
HDPE/$cSiO_2$	21.4 ± 3.1	29.7 ± 2.1	805 ± 33	702 ± 35	32 ± 3
HDPE/MMT	21.0 ± 1.8	23.6 ± 2.5	833 ± 47	611 ± 40	39 ± 3
HDPE/org-MMT	20.9 ± 1.2	25.1 ± 2.2	639 ± 30	618 ± 33	40 ± 4

TEM micrographs show the dark lines of MMT layers. In nanocomposites containing untreated MMT, the dispersed particles into HDPE matrix have sizes close to 10 nm width and 1000 nm length. Comparing Figure 1(c,d), it can be seen that the org-MMT has a better dispersion in the HDPE matrix but no exfoliated nanoparticles can be detected. These results show that the intercalation effect of HDPE is limited because of its nonpolar character. In most cases by using MMT as nanoparticles, the synthesis of polymer/MMT nanocomposites is reported mainly via melt-direct intercalation since it is the most promising method, easily applied in industry and does not require any solvents. However, since HDPE does not include any polar group in its backbone, a homogeneous dispersion of clay minerals in its matrix is not achieved even when the clay is organically modified. A better dispersion was reported when PE-*g*-MA copolymer was used simultaneously during melt mixing.[23] Aggregates are also observed in nanocomposites containing MWCNTs [Fig. 1(e)], which is very usual in polyolefins.[24] This happens because MWCNTs contain some surface carboxyl and hydroxyl groups, which can participate to hydrogen bond interactions between each other.

Mechanical properties

Nanoparticles consist of very small particles in the range of nanoscale. Thus, they have large aspect ratio and when incorporated into polymer it is expected to increase the mechanical properties, even at low filler loading (2.5–5 wt %). As far as the toughening mechanism is concerned, it is generally believed that cavitations of the polymer matrix surrounding the rigid inorganic particles can promote extensive shear yielding, thus increasing the energy absorbed in highly dissipative phenomena. All the mechanical properties of the studied nanocomposites are presented in Table I. From stress–strain curves, it is observed that nanocomposites, except HDPE/MWCNTs, exhibit the typical cold-drawn behavior since cold drawing appeared before the final break of the specimen. This was also reflected to the elongation at break, which is very high in all nanocomposites except those containing MWCNTs. Also, it can be seen that the values of tensile strength at yield point of all nanocomposites are very close to the corresponding HDPE. Thus, no clear conclusion concerning the adhesion between HDPE matrix and nanoparticles can be derived.

In the case of tensile strength at break, there are some remarkable differences. Nanocomposites containing MWCNTs and MMT have lower tensile strength than neat HDPE and only when SiO_2 was used, there was a small improvement of tensile strength. MMT nanoparticles were reported to cause a reduction in tensile strength.[25] HDPE is a nonpolar hydrophobic polymer and thus strong interactions with polar hydrophilic fillers, such as those used, cannot take place. For this reason, coated nanoparticles can be used to increase the adhesion with HDPE matrix. Lazzeri et al.[26] concluded that the addition of coated nano-sized calcium carbonate could compensate the decrease of the tensile properties compared with the uncoated precipitate calcium carbonate. The results of their study show that addition of fatty acids, such as stearic acid, can be a good way to achieve a uniform dispersion with suitable adhesion. However, in the prepared nanocomposites when coated and uncoated SiO_2 were used (such an) similar improvement was not observed. On the contrary, the nanocomposites containing coated SiO_2 present lower tensile strength than the uncoated. Such a behavior was also observed in our previous study when these nanoparticles were used in polypropylene (PP).[20] This reduction can be attributed to higher agglomerates that these nanoparticles create in the polymer matrix, as was found also by TEM micrographs.

The observations for impact strength values were also similar to this. The addition of nanoparticles into HDPE matrix results in the reduction of impact strength, in agreement with the already published studies in HDPE reinforced with nanoparticles. The low toughness of the clay-reinforced polyethylene, compared with neat polyethylene, is related to the crystal structure and the interfacial interaction between the filler and the polymer matrix.[27] Thus, the addition of clay into polyethylene decreases the impact strength for the entire temperature range of Izod impact tests. In this study, it was reported that the fracture of polyethylene initiates with crazing, whereas the fracture initiation and propagation of clay-polyethylene nanocomposite are characterized by stretching of fibrils (fibrillation) interdispersed with microvoids. To the exception of the above-discussed mechanical properties, Young's modulus seems to have a substantial increase in all nanocomposites, compared with the corresponding HDPE. The increased stiffness is due to the reinforcement effect of the nanofillers in the polymer matrix.[28,29]

Dynamic mechanical analysis

Storage and loss modular spectra of HDPE/nanocomposites containing 2.5 wt % of different nanoparticles are shown in Figures 2 and 3, respectively. Examining the storage modulus of these nanocomposites, a constantly falling trend over the temperature range can be observed, while the major transition seems to be detected in the rubbery stage between 20 and 60°C. Storage modulus of all nanocomposites is higher compared to the corresponding

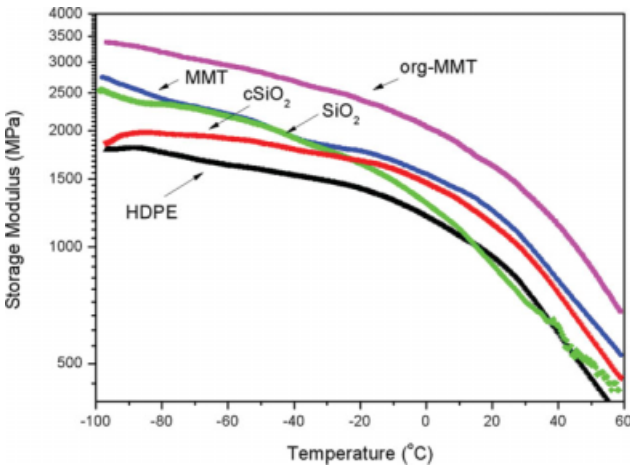

Figure 2 Storage modulus (E′) of HDPE nanocomposites. [Color figure can be viewed in the online issue, which is available at www.intersciene.wiley.com.]

modulus of HDPE, which indicates increased stiffness of these materials. This was also verified from Young's modulus measured from mechanical properties. It is evident from Figure 2 that there is a remarkable increase in the modulus of neat HDPE with the incorporation of nanoparticles. This is probably due to increase in the stiffness of the matrix with the reinforcing effect imparted by the nanoparticles that allowed a greater degree of stress transfer at the interface.

Concerning the loss modulus in the case of neat HDPE, a very slight loss modulus peak around −90°C and a more intense around 30°C are recorded (Fig. 3). In the literature, it was reported that HDPE shows two relaxation peaks at −110°C (γ), which is attributed to the glass transition temperature and at 60–80°C (a), respectively.[30] The b transition is not visible in HDPE because of the absence of the branches and is only observed in LDPE. In the loss modulus curve for neat HDPE, a transition can be

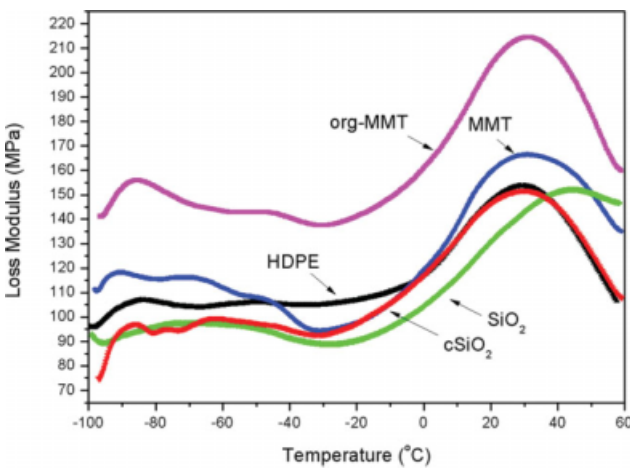

Figure 3 Loss modulus (E″) of HDPE nanocomposites. [Color figure can be viewed in the online issue, which is available at www.intersciene.wiley.com.]

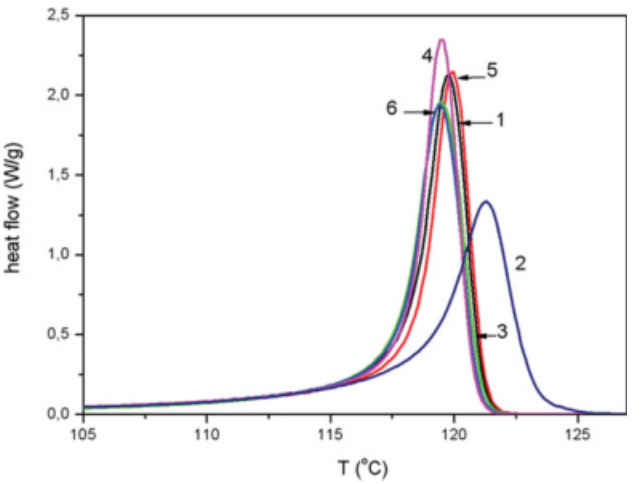

Figure 4 Exothermic melt crystallization peak of HDPE nanocomposites. (1) HDPE, (2) HDPE/MWCNTs, (3) HDPE/org-MMT, (4) HDPE/MMT, (5) HDPE/SiO_2, (6) HDPE/$cSiO_2$. [Color figure can be viewed in the online issue, which is available at www.intersciene.wiley.com.]

seen as a broad peak with maximum at 31°C (Fig. 3). The α relaxation is associated with the chain segment mobility in the crystalline phases, which is probably due to reorientation of defect areas in the crystals and is thought to be dependent on the lamellar fold surface morphology. According to the literature, each 1% increment in crystallinity will shift α by about 0.5°C.[30] Additionally, it has been reported[31] that the α-relaxation was not detected in samples with less than 40% crystallinity. In our case, since the crystallinity of HDPE is lower in all nanocomposites (it will be discussed further), the shift of α-relaxation to slightly higher values should be attributed to the reinforcing effect of nanoparticles.

Thermal analysis

The melting (T_m) as well as the crystallization temperature (T_c) of the HDPE nanocomposites were also measured. The melting point of neat HDPE is recorded at 127°C and the heat of fusion is 148.8 J/g, while the melting points of HDPE with nanocomposites were also similar with the appeared differences being negligible (0.1–0.3°C). Sahebian et al.[32] reported that nanosized calcium carbonate in HDPE/$CaCO_3$ nanocomposites present a significant effect on crystallinity, crystallization rates, melting point, and heat of melting of HDPE. Such a behavior was also observed using SiO_2 and MMT where the crystallization rates in both nanocomposites are higher, compared with neat HDPE, but the degree of crystallinity was reduced.[23,33] Reductions were also observed in heat of fusion for HDPE nanocomposites of the present study containing pristine MMT nanoparticles (139.7 J/g) and organically modified MMT (141.3 J/g). This is similar to the heat of fusion

in nanocomposites containing MWCNTs (140.6 J/g), whereas the most remarkable reductions in heat of fusion were recorded in nanocomposites containing SiO_2 (136.6 J/g) and coated SiO_2 (137 J/g). Some small differences, as in the case of melting points, were also observed in crystallization temperatures.

HDPE crystallizes at 119.5°C after cooling from its melt. As can be seen in Figure 4 all nanocomposites, except those with MWCNT, have similar crystallization temperatures even though it is well known that nanoparticles can act as nucleating agents. The differences in crystallization temperatures range between 0.1 and 0.4°C, which are in the area of experimental error. Only in the case when MWCNTs were used as additives, there is a substantial difference, close to 2.5°C, and this nanocomposite HDPE crystallizes more quickly than the others. This is probably due to the higher surface area that MWCNTs have in contact with HDPE matrix and MWCNTs induce a heterogeneous nucleation effect. However, from XRD studies, no effect was found on the crystalline structure of HDPE. XRD patterns show three strong peaks at $2\theta = 19.33$, 21.46, and 23.82°. The intensity of these peaks, as well as their position, remain unaffected for all nanocomposites.

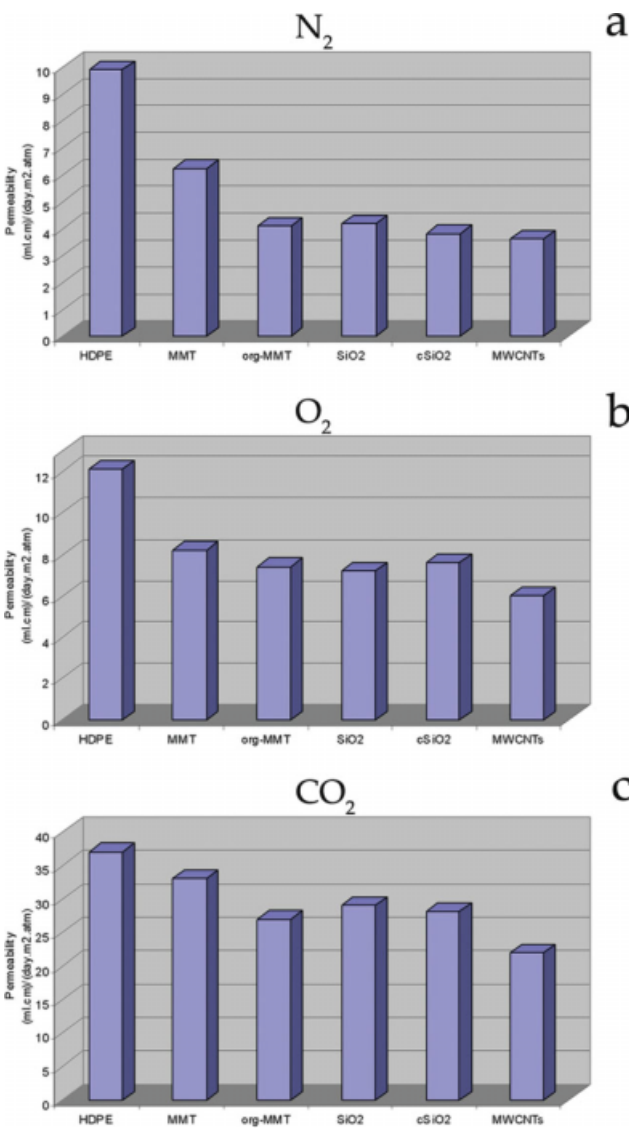

Figure 5 Permeability of N_2, O_2, and CO_2 from HDPE nanocomposites containing 2.5 wt % of different nanoparticles. [Color figure can be viewed in the online issue, which is available at www.intersciene.wiley.com.]

Gas permeability

One of the most important advantages of nanoparticles' insertion into polymer matrices is the enhancement of gas barrier properties of the final material. Nanoparticles are impermeable anisotropic materials that force the gas molecules to diffuse around them in a more complicated way. The tortuous pathway is increased and the permeability of the nanocomposites is reduced compared with neat polymers. This was also found for other polymer nanocomposites with PP.[24,34,35] In this study, the gas transmission rates (TR) of different gases such as O_2, N_2, and CO_2 through each HDPE nanocomposite film were calculated using the following equation:

$$\mathrm{TR} = \frac{(273 \times \mathrm{p} \times \mathrm{V})(24 \times 10^4)}{\mathrm{A} \times \mathrm{T} \times \mathrm{P}} \quad (1)$$

where TR is the gas transmission rate calculated in $mL/m^2 \cdot day \cdot atmosphere$, p is the rate of pressure change in the capillary pipe (cmHg/h), V is the total free volume in the sample shell (5 mL), A the surface of the sample (23.77 cm^2), T the temperature at which the experiment is carried out (25°C), and P the pressure difference at the beginning of the experiment in cmHg, which can be considered as 76 cmHg. TRs can be easily converted to gas permeability using the equation:

$$P = \mathrm{TR} \times l \quad (2)$$

where l is the film thickness.

The factors that affect the gas permeability of a polymer are the degree of crystallinity, the existence of polar groups, the structure compactness, and the used fillers. However, in the studied samples the heat of fusion (ΔH_m) was slightly decreased in all nanocomposites. Furthermore, HDPE chemical structure remains unaffected since no compatibilizers or other additives were used. Thus, any change into gas permeability should be attributed only to the kind of nanoparticles used. As can be seen from Figure 5, the permeability of the studied gases is reduced by the addition of the different nanoparticles, compared with the neat HDPE film. However, this reduction is more pronounced in O_2 and N_2, whereas the reduction is in lower magnitude in the

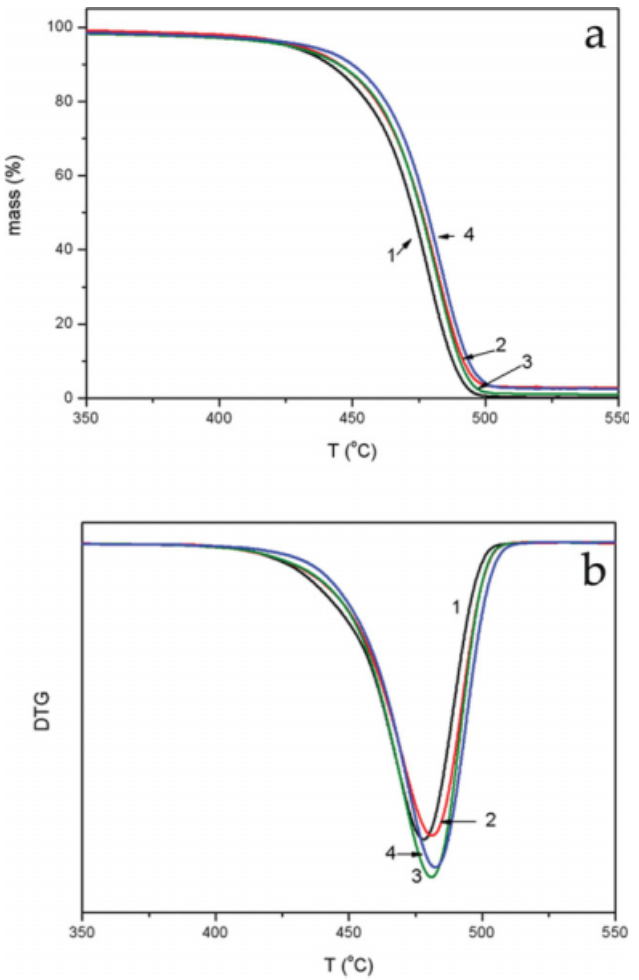

Figure 6 (a) Mass loss (%) versus temperature and (b) derivative mass loss (DTG) versus temperature with a heating rate β = 10°C/min for all studied samples. (1) HDPE, (2) HDPE/MMT, (3) HDPE/$cSiO_2$, (4) HDPE/MWCNTs. [Color figure can be viewed in the online issue, which is available at www.intersciene.wiley.com.]

case of CO_2. Neat HDPE has an N_2 permeability of 9.7 mL cm/day m^2 atm and this is reduced to 3.33 mL cm/day m^2 atm after the addition of 2.5 wt % MWCNTs. This nanocomposite has the lowest permeability whereas the others are slightly higher. The nanocomposite containing MMT has comparatively, the higher N_2 permeability from all the studied nanocomposites, and this trend is also valid for O_2 [Fig. 5(b)]. It is well known that such MMT nanoparticles are considered impenetrable by gas molecules. Thus, it is believed that the addition of MMT in the matrix resin would enhance its barrier properties by forcing the gas molecules to follow a more tortuous path as they diffuse through the material, retarding the progress of the phenomenon. This has been observed in many polymer/layered silicate nanocomposites as well as in iPP using fumed silica nanoparticles.[36,37] However, in the case of MMT, as was found from SEM, these nanoparticles were not exfoliated and for this reason a fine dispersion of clay particles was not achieved. Thus, an effective gas barrier increase was not possible. Similar behavior was also reported by Zhong et al.[16] However, Osman et al.[17] found that in HDPE/MMT nanocomposites oxygen permeability reduces by increasing the *d*-spacing. Thus, it seems that when MMT were used as nanofillers the oxygen permeability can, substantially, be reduced when MMT is exfoliated. In the case that CO_2 was used as gas, as can be seen, the gas permeation rates from all studied nanocomposites are very high. This is because CO_2 also has a high solubility in many polymers and for this reason its permeability is highest compared with the other two gases [Fig. 5(c)]. However, even for this gas, a slight reduction in permeability was observed in all nanocomposites, with a similar trend as in the cases of O_2 and N_2.

Thermal degradation study of HDPE nanocomposites

Thermal degradation of HDPE and HDPE/nanocomposites was studied by determining their mass loss during heating in a nitrogen atmosphere. In Figure 6, the mass loss and the derivative mass loss (derivative thermogravity (DTG)) curves of all studied samples are presented, at a heating rate of 10°C/min.

From the thermogravimetric curves, it can be seen that HDPE, and the samples with different nanoparticles, present a relatively good thermostability since, for example, the maximum mass loss, occurred until 275°C, is 1% for the sample HDPE-$cSiO_2$. As it can be seen from the peak of the first derivative, the temperature at which the HDPE decomposition rate

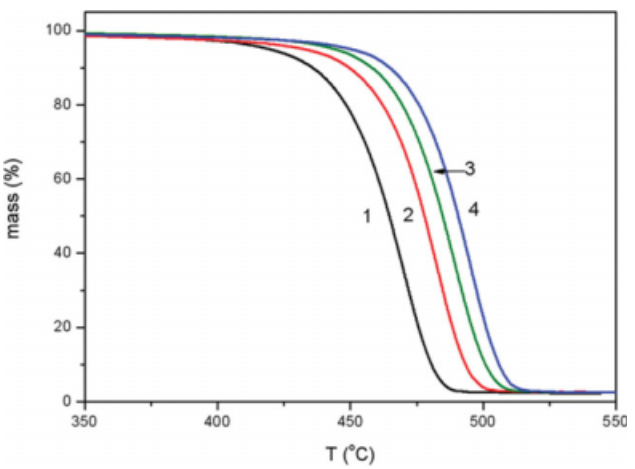

Figure 7 Mass loss (%) curves of sample containing MWCNTs at different heating rates. (1) β = 5, (2) β = 10, (3) β = 15, (4) β = 20 °C/min. [Color figure can be viewed in the online issue, which is available at www.intersciene.wiley.com.]

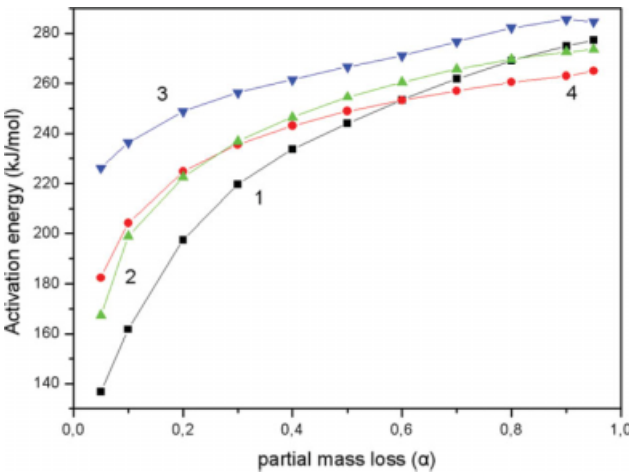

Figure 8 Dependence of the activation energy (E) on the degree of the partial mass loss (α), as calculated with OFW method for the different nanocomposites. (1) HDPE, (2) HDPE-MMT, (3) HDPE-cSiO$_2$, (4) HDPE-MWCNTs. [Color figure can be viewed in the online issue, which is available at www.intersciene.wiley.com.]

is highest is, T_p = 478.1°C, for a heating rate of 10°C/min. The corresponding temperatures are T_p = 481.2, 481, and 482.4°C for HDPE/MMT, HDPE/cSiO$_2$, and HDPE/MWCNTs, respectively. These values present a small but significant increase at the highest decomposition rate temperature due to the incorporation of the nanoparticles.

The shape of the mass loss curve is the same for all samples. To analyze more thoroughly the effect of the type of nanoparticles on the degradation mechanism of HDPE, it is important that the kinetic parameters (activation energy E and preexponential factor A) and the conversion function $f(\alpha)$ to be evaluated. The relationship between kinetic parameters and conversion (α), partial mass loss, can be found using the mass loss curves recorded in the thermogravimetric measurements. The degradation for all the samples was studied through nonisothermal measurements at different heating rates (5, 10, 15, and 20°C/min). In Figure 7, the mass loss at different heating rates for HDPE/MWCNTs is presented as a characteristic example.

For the calculation of the activation energies, all heating rates have been used and they were estimated using the Ozawa, Flynn, and Wall (OFW),[38–41] Friedman,[42,43] and Kissinger[44] methods for comparison reasons. At first, the isoconversional OFW method was used to calculate the activation energy for different conversion values. Second, the Friedman method was used by plotting $\ln(d\alpha/dT)$ against $1/T$ for a constant α value and the activation energy was calculated. The results and the differences among the studied samples in the activation energy, as predicted with OFW and Friedman methods, can be seen in Figures 8 and 9 for all the samples.

From the plots, it can be seen that although the shape of the curves is almost the same, significant differences can be recognized in the activation energy values for the same value of partial mass loss. The differences in the values of E calculated by the OFW and Friedman methods can be explained by a systematic error due to improper integration. The method of Friedman uses instantaneous rate values being, therefore, very sensitive to experimental noise. With OFW method, the equation used is derived assuming constant activation energy with the introduction of a systematic error in the estimation of E in the case that E varies with α, an error that can be estimated by comparison with the Friedman results.[45] From these calculations, the variation of the activation energy values can be estimated. The differences of the activation energy as predicted with OFW and Friedman methods among the studied samples can be seen in Figures 8 and 9.

The activation energy was also calculated with the Kissinger's method for all the studied samples. In Figure 10, the Kissinger plots for HDPE and HDPE-MWCNTs samples can be seen. These values (Table II) are in the same area with the values calculated using the OFW and Friedman methods.

It is deduced from Figures 8 and 9 that the dependence of E on α value can be discriminated in to two distinct regions, the first for values of α almost up to 0.2, in which E presents a rapid increase, and the second for α >0.2 in which E presents more or less a slight increase. The dependence of the activation energy of the partial mass loss, in the first region, is much stronger for the HDPE samples than that for the

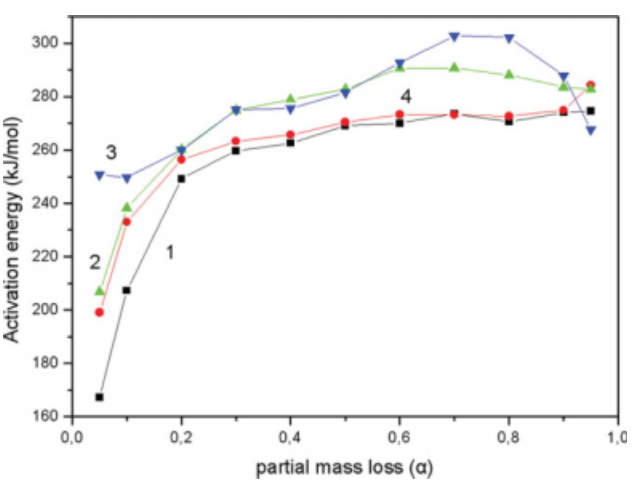

Figure 9 Dependence of the activation energy (E) on the degree of the partial mass loss (α), as calculated with Friedman's method for the different nanocomposites. (1) HDPE, (2) HDPE/MMT, (3) HDPE/cSiO$_2$, (4) HDPE/MWCNTs. [Color figure can be viewed in the online issue, which is available at www.intersciene.wiley.com.]

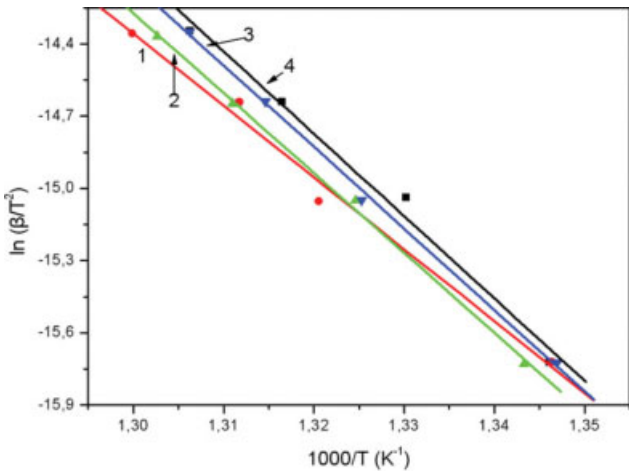

Figure 10 Kissinger's method for HDPE nanocomposites. (1) HDPE, (2) HDPE/ MWCNTs, (3) HDPE/MMT, (4) HDPE/cSiO$_2$. [Color figure can be viewed in the online issue, which is available at www.intersciene.wiley.com.]

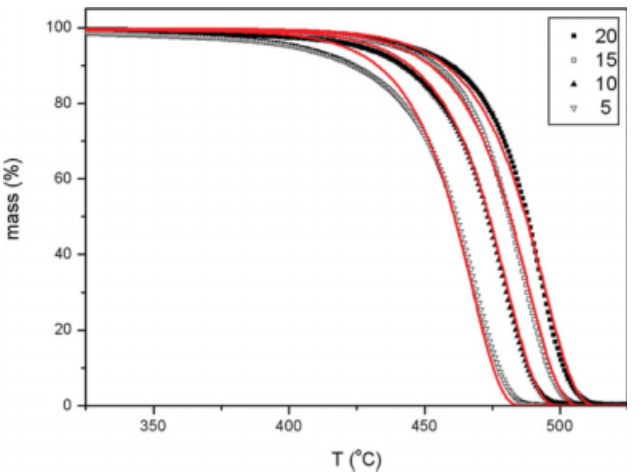

Figure 11 Mass loss (%) of HDPE samples and fitting curves with the Cn reaction model for different heating rates β = 5, 10, 15, and 20°C/min. [Color figure can be viewed in the online issue, which is available at www.intersciene.wiley.com.]

other HDPE nanocomposites. This dependence of E on α is an indication of a complex reaction with the participation of at least two different mechanisms, from which one has quite a small effect on mass loss. Examining the dependence of E on α value for the studied HDPE nanocomposites, it is concluded that this dependence of thermal decomposition of HDPE remains almost the same. According to the literature,[46–56] single reaction mechanism has been used for the kinetics analysis of HDPE degradation and the calculated activation energies present a lot of differences. The models that have been used are the first order (F1), the nth order (Fn), and the phase boundary controlled reaction-contracting area (R^2). These reaction models were examined also for the HDPE and HDPE nanocomposites of the present study.[57,58] To determine the nature of the mechanism, through the comparison of the experimental and theoretical data, it is considered that the degradation of the HDPE can be described only by a single mechanism that corresponds to the main mass loss, without presuming the exact mechanism. This model has also been applied in our previous studies in polyesters as well as in iPP but without any success, since the differences between the theoretical and experimental data were very high.[59–63] The quality of the fitting with these two models was not acceptable after their application in HDPE and its nanocomposites (data not shown), as was expected. To improve it, 16 different reaction models were examined. The form of the conversion function, given by the best fitting for the HDPE and HDPE nanocomposites, is the mechanism of autocatalysis n-order (Cn) $f(\alpha) = (1 - \alpha)^n(1 + K_{cat}X)$, where K_{cat} is a constant and X the reactants. In Figures 11 and 12, the results of this fitting can be seen for HDPE and one of the HDPE nanocomposites.

Comparing the results of the fitting with the Fn and Cn models for the same samples, it is obvious that the Cn model fits the experimental data better, especially at the end of the mass loss. On the other hand, comparing the results of the fitting for the

TABLE II
Activation Energy (E) as Calculated with Kissinger's Method

Sample	Activation Energy (kJ/mol)
HDPE	252.7
HDPE/MWCNTs	265.9
HDPE/MMT	276.4
HDPE/cSiO$_2$	281.1

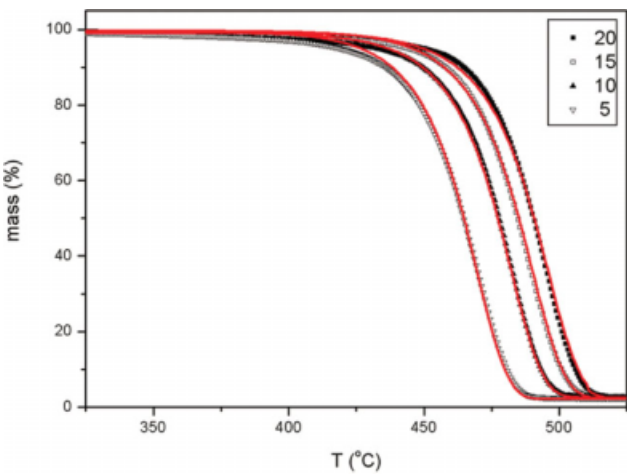

Figure 12 Mass loss (%) of HDPE/MWCNTs samples and fitting curves with the Cn reaction model for different heating rates β = 5, 10, 15, and 20°C/min. [Color figure can be viewed in the online issue, which is available at www.intersciene.wiley.com.]

TABLE III
Activation energy, preexponential Factor and Reaction Order for Fn and Cn Reaction Models

Sample	Activation energy (kJ/mol)	Preexponential factor (s^{-1})	Reaction order (n)
Reaction model Fn			
HDPE	245.2	14.9	0.39
HDPE/MWCNTs	256.2	15.6	0.40
HDPE/MMT	255.7	15.6	0.45
HDPE/$cSiO_2$	266.9	16.4	0.48
Reaction model Cn			
HDPE	239.1	14.3	0.74
HDPE/MWCNTs	245.7	14.7	0.9
HDPE/MMT	251.6	15.2	0.68
HDPE/$cSiO_2$	262.4	16.0	0.72

TABLE IV
Activation Energy, preexponential Factor and Reaction Order of HDPE Nanocomposites After Fitting with Two Reaction Mechanisms

Sample	Activation energy (kJ/mol)	Preexponential factor (s^{-1})	Reaction order (n)	log K_{cat}
First reaction mechanism - Reaction model Cn				
HDPE	140.0	7.9	0.27	−4.7*
HDPE/MWCNTs	200.0	12.3	0.69	−7.2*
HDPE/MMT	175	10.5	0.77	−28.6*
HDPE/$cSiO_2$	230.0	14.6	1.23	−18.2*
Second reaction mechanism - Reaction model Cn				
HDPE	260.0	15.8	1.01	0.47
HDPE/MWCNTs	270.0	15.7	1.06	0.44
HDPE/MMT	285.0	17.6	0.98	0.22
HDPE/$cSiO_2$	290.0	18.0	1.03	0.30

HDPE and the HDPE-MWCNTs samples with the Cn model, it is obvious that the quality of the fitting for the nanocomposite is better than that for the HDPE sample. Small divergences appeared only at the first area of the mass loss and this divergence is large mainly at the lower heating rate of 5°C/min. This conclusion is the same for the other nanocomposites. The calculated values of the activation energy and the reaction order for all the studied samples for the two reaction models (Fn, Cn) are presented in Table III. As can be seen, by both used models, the activation energies of HDPE/nanocomposites are higher than that for neat HDPE. This is a further proof that nanoparticles increase thermal stability of HDPE.

Because the quality of the fitting for the HDPE is not yet in an acceptable level and using the conclusions from the dependence of the activation energy on the partial mass loss, two reaction mechanisms instead of one might be used to improve the quality of the fitting. For the determination of the mechanism at the first mass loss area for HDPE as well as for its nanocomposites, the following are assumed: (a) the two mechanisms are consecutive and (b) this mechanism, which we try to identify, corresponds to a small mass loss, according to the experimental results. The fitting with two consecutive mechanisms leads to a remarkable improvement in the fitting of the experimental results with the theoretical ones. One characteristic example is presented in Figure 13 for HDPE/$cSiO_2$ sample. The results are similar for the HDPE and the other three nanocomposites.

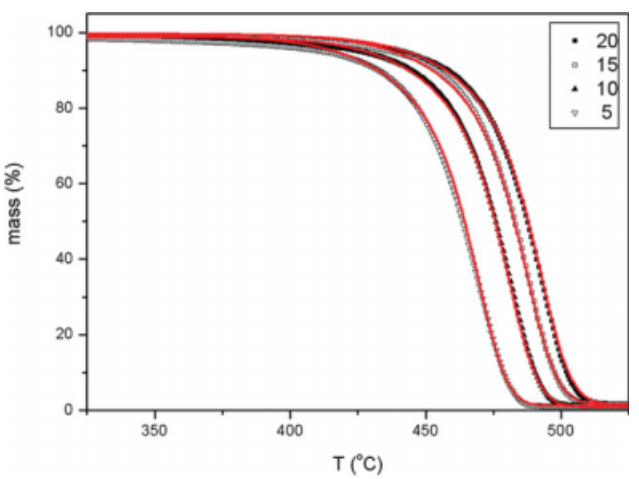

Figure 13 Mass loss (%) of HDPE/$cSiO_2$ samples and fitting curves for different heating rates β = 5, 10, 15, and 20°C/min and for two reaction mechanisms. [Color figure can be viewed in the online issue, which is available at www.intersciene.wiley.com.]

The form of the conversion function, obtained by the best fitting, with a regression factor at least 0.9998, is the mechanism of autocatalysis *n*-order $f(\alpha) = (1 - \alpha)^n(1 + K_{cat}X)$ for all the studied samples. In this stage of identification, for the best possible results we left the parameters (*E*, *A*, and *n*) of the second mechanism to be recalculated. The theoretical data fit very well the experimental data in the first area of small mass loss. From these curves, there is no evidence that we must use another mechanism to further improve the fitting. So, we can conclude that to describe the thermal degradation of HDPE and its studied nanocomposites, two consecutive mechanisms of *n*th order autocatalysis have to be considered. The results from all the different samples are summarized in Table IV. For the region of small mass loss, it is obvious that the parameter log K_{cat} has large negative values for all the studied samples so the parameter K_{cat} does not play a significant role in the quality of the fitting, and for this reason the reaction model Fn can be used instead of Cn. The values of the activation

energy, the preexponential factor, and the reaction order of the Fn model are the same with that of the reaction model Cn.

CONCLUSIONS

In the prepared HDPE nanocomposites, different nanoparticles were added in an amount 2.5 wt % to compare their effect on polymer properties. Those nanocomposites containing coated and uncoated SiO_2 have the best dispersion, which was also reflected in the mechanical properties. Because of the lack of exfoliation, tensile tests on all nanocomposites containing MMT indicated that incorporation of nanoclay into HDPE reduces tensile strength. Greater enhancement of the tensile or Young's modulus was observed for all nanocomposites. Melting point and crystallization temperatures were unaffected from the addition of different nanoparticles but heat of fusion was slightly reduced. However, even after this decrease of crystallinity, all nanocomposites exhibited decreased gas permeability by O_2, N_2, and CO_2. An additional enhancement was also observed to the thermal stability of nanocomposites. By using different kinetic models, it was found that the degradation of HDPE can be described by two autocatalysis *n*th order mechanisms. Similar mechanisms can also be used with the HDPE nanocomposites, which however have higher activation energies from neat HDPE.

References

1. Galli, P.; Vecellio, G. J Appl Polym Sci Part A Polym Chem 2004, 42, 396.
2. Nielsen, L. E.; Landel, R. F.; Nielsen, L. E., Landel, R. F., Eds. Mechanical Properties of Polymers and Composites, 2nd ed.; Marcel Dekker Inc.: New York, 1994.
3. Tjong, S. C. Mater Sci Eng R 2006, 53, 73.
4. Zhang, M. Q.; Rong, M. Z.; Zhang, H. B.; Friedrich, K. Polym Eng Sci 2003, 43, 490.
5. Ou, Y. C.; Yang, F.; Yu, Z. Z. J Polym Sci Part B Polym Phys 1998, 36, 789.
6. Wang, K. H.; Koo, C. M.; Chung, I. J. J Appl Polym Sci 2003, 89, 2131.
7. Lee, Y. H.; Park, B.; Sain, M.; Kontopoulou, M.; Zheng, W. J Appl Polym Sci 2007, 105, 1993.
8. Chu, D.; Nguyen, Q.; Baird, D. G. Polym Comp 2007, 28, 499.
9. Wang, K. H.; Xu, M.; Choi, Y. S.; Chung, I. J. Polym Bull 2001, 46, 499.
10. Min, K. D.; Kim, M. Y.; Choi, K. Y.; Lee, J. H.; Lee, S. G. Polym Bull 2006, 57, 101.
11. Filippi, S.; Marazzato, C.; Magagnini, P.; Famulari, A.; Arosio, P.; Meille, S. V. Eur Polym J 2008, 44, 987.
12. Lee, J. H.; Kim, S. K.; Kim, N. H. Scr Mater 2006, 55, 1119.
13. Trujillo, M.; Arnal, M. L.; Müller, A. J.; Laredo, E.; Bredeau, S. T.; Bonduel, D.; Dubois, P. H. Macromolecules 2007, 40, 6268.
14. Wu, F.; He, X.; Zeng, Y.; Cheng, H. M. Appl Phys A 2006, 85, 25.
15. Zou, Y.; Feng, Y.; Wang, L.; Liu, X. Carbon 2004, 42, 271.
16. Zhong, Y.; Janes, D.; Zheng, Y.; Hetzer, M.; Kee, D. D. Polym Eng Sci 2007, 7, 1101.
17. Osman, M. A.; Rupp, J. E. P.; Suter, U. W. J Mater Chem 2005, 15, 1298.
18. Pavlidou, E.; Bikiaris, D.; Vassiliou, A.; Chiotelli, M.; Karayannidis, G. J Phys Conf Ser 2005, 10, 190.
19. Bikiaris, D.; Vassiliou, A.; Pavlidou, E.; Karayannidis, P. Eur Polym J 2005, 41, 1965.
20. Bikiaris, D. N.; Papageorgiou, G. Z.; Pavlidou, E.; Vouroutzis, N.; Palatzoglou, P.; Karayannidis, G. P. J Appl Polym Sci 2006, 100, 2684.
21. Liu, Y.; Kontopoulou, M. Polymer 2006, 47, 7731.
22. Kontou, E.; Niaounakis, M. Polymer 2006, 47, 1267.
23. Gopakumar, T. G.; Lee, J. A.; Kontopoulou, M.; Parent, J. S. Polymer 2002, 43, 5483.
24. Bikiaris, D.; Vassiliou, A.; Chrissafis, K.; Paraskevopoulos, K. M.; Jannakoudakis, A.; Docoslis, A. Polym Degrad Stab 2008, 93, 952.
25. Osman, M. A.; Rupp, J. E. P.; Suter, U. W. Polymer 2005, 46, 1653.
26. Lazzeri, A.; Zebarjad, S. M.; Pracella, M.; Cavalier, K.; Rosa, R. Polymer 2005, 46, 844.
27. Tanniru, M.; Yuan, Q.; Misra, R. D. K. Polymer 2006, 47, 2133.
28. Kanagaraj, S.; Varanda, F. R.; Zhil'tsova, T. V.; Oliveira, M. S. A.; Simões, J. A. O. Comp Sci Techn 2007, 67, 3071.
29. Tang, W.; Santare, M. H.; Advani, S. G. Carbon 2003, 41, 2779.
30. John, B.; Varughese, K. T.; Oommen, Z.; Potschke, P.; Thomas, S. J Appl Polym Sci 2003, 87, 2083.
31. Stadler, F. J.; Kaschta, J.; Münstedt, H. Polymer 2005, 46, 10311.
32. Sahebian, S.; Zebarjad, S. M.; Sajjadi, S. A.; Sherafat, Z.; Lazzeri, A. J Appl Polym Sci 2007, 104, 3688.
33. Jiasheng, Q. J Mater Sci 2003, 38, 2299.
34. Vassiliou, A.; Bikiaris, D.; Chrissafis, K.; Paraskevopoulos, K. M.; Stavrev, S. Y.; Docoslis, A. Comp Sci Techn 2008, 68, 933.
35. Vassiliou, A.; Bikiaris, D.; Pavlidou, E. React Eng 2007, 1, 488.
36. Mittal, V. J Appl Polym Sci 2008, 107, 1350.
37. Mirzadeh, A.; Kokabi, M. Eur Polym J 2007, 43, 3757.
38. Ozawa, T. Bull Chem Soc 1965, 38, 1881.
39. Flynn, J. H.; Wall, L. A. J Res Natl Bur Stand Phys Chem 1966, 70, 487.
40. Flynn, J. H.; Wall, L. A. Polym Lett 1966, 4, 232.
41. Ozawa, T. J Therm Anal 1970, 2, 301.
42. Friedman, H. L. J Polym Sci Part C 1964, 6, 183.
43. Friedman, H. L. J Polym Lett 1966, 4, 323.
44. Kissinger, H. E. Anal Chem 1957, 29, 1702.
45. Vyazovkin, S. J Comput Chem 2001, 22, 178.
46. Wu, C. H.; Chang, C. Y.; Hor, J. L.; Shih, S. M.; Chen, L. W.; Chang, F. W. Waste Manag 1993, 13, 221.
47. Knumann, R.; Bockhorn, H. Comput Sci Tech 1994, 101, 285.
48. Bockhorn, H.; Hornung, A.; Hornung, U.; Schawaller, D. J Anal Appl Pyrol 1999, 48, 93.
49. Bockhorn, H.; Hornung, A.; Hornung, U. J Anal Appl Pyrol 1999, 50, 77.
50. Park, J. W.; Oh, S. C.; Lee, H. P.; Kim, H. T.; Yoo, K. O. Polym Degad Stab 2000, 67, 435.
51. Ballice, A. Fuel 2001, 80, 1923.
52. Yang, J.; Miranda, R.; Roy, C. Polym Degrad Stab 2001, 73, 455.
53. Araujo, A. S.; Fernandes, V. J.; Fernandes, J. G. J. T. Thermochim Acta 2002, 55, 392.
54. Gao, Z.; Amasaki, I.; Nakada, M. J Anal Appl Pyrol 2003, 67, 1.

55. Kim, S.; Jang, E. S.; Shin, D. H.; Lee, K. H. Polym Degrad Stab 2004, 85, 799.
56. Sinfronio, F. S. M.; Santos, J. C. O.; Pereira, L. G.; Souza, A. G.; Conceicao, M. M.; Fernandes, V. J.; Fonseca, V. M. J Therm Anal Cal 2005, 79, 393.
57. Opfermann, J.; Wilke, G.; Ludwig, W.; Hagen, S.; Gebhardt, M.; Kaisersberger, E. Thermochim Acta 1991, 187, 151.
58. Kaisersberger, E.; Opfermann, J. Laborpraxis 1992, 4, 360.
59. Chrissafis, K.; Paraskevopoulos, K. M.; Bikiaris, D. N. Thermochim Acta 2005, 435, 142.
60. Chrissafis, K.; Paraskevopoulos, K. M.; Bikiaris, D. N. Polym Degrad Stab 2006, 91, 60.
61. Zorba, T.; Chrissafis, K.; Paraskevopoulos, K. M.; Bikiaris, D. N. Polym Degrad Stab 2007, 92, 222.
62. Chrissafis, K.; Antoniadis, G.; Paraskevopoulos, K. M.; Vassiliou, A.; Bikiaris, D. N. Comp Sci Techn 2007, 67, 2165.
63. Chrissafis, K.; Paraskevopoulos, K. M.; Stavrev, S. Y.; Docoslis, A.; Vassiliou, A.; Bikiaris, D. N. Thermochim Acta 2007, 465, 6.